

The $\phi(1020) \rightarrow \pi^0\pi^0\gamma$ decay*

M.N. Achasov, S.E. Baru, K.I. Beloborodov, A.V. Berdyugin, A.V. Bozhenok,
 A.D. Bukin, D.A. Bukin, S.V. Burdin, T.V. Dimova, A.A. Drozdetsky,
 V.P. Druzhinin, M.S. Dubrovin, I.A. Gaponenko, V.B. Golubev, V.N. Ivanchenko†,
 A.A. Korol, I.A. Koop, S.V. Koshuba, G.A. Kukartsev, A.A. Mamutkin,
 E.V. Pakhtusova, A.A. Salnikov, S.I. Serednyakov, V.V. Shary, Yu.M. Shatunov,
 V.A. Sidorov, Z.K. Silagadze, A.N. Skrinisky, A.A. Valishev, A.V. Vasiljev

Budker Institute of Nuclear Physics, Novosibirsk, 630090, Russia

Abstract

In the SND experiment at VEPP-2M e^+e^- collider the $\phi(1020) \rightarrow \pi^0\pi^0\gamma$ decay was studied and its branching ratio was measured: $B(\phi \rightarrow \pi^0\pi^0\gamma) = (1.221 \pm 0.098 \pm 0.061) \cdot 10^{-4}$. It was shown, that $f_0(980)\gamma$ intermediate state dominates in this decay and the $f_0(980)$ -meson parameters were obtained.

*PACS:*12.39.Mk, 13.40.Hq, 14.40.Cs

Keywords: scalar, vector, decay, four-quark, gamma, radiative

1 Introduction

The first work to search for the decay $\phi \rightarrow \pi^0\pi^0\gamma$ was performed in 1987 [1, 2]. The observation of this decay based on analysis of the data of the PHI96 experiment [3] was reported in 1997 [4, 5] by the SND detector [6]. Observed decay rate of about 10^{-4} was unexpectedly high and it was also shown that $f_0(980)\gamma$ intermediate state dominates in this decay. Later these results were confirmed by the CMD-2 experiment [7].

In this work results are presented of a new experimental study of the process

$$e^+e^- \rightarrow \phi \rightarrow \pi^0\pi^0\gamma \quad (1)$$

based on complete SND statistics of about $2 \cdot 10^7$ produced ϕ mesons. The experiments were carried out at VEPP-2M e^+e^- collider in Novosibirsk. The total integrated luminosity collected in PHI96 [3] and PHI98 [8] experiments was $4 pb^{-1}$ in 20 energy points and $8 pb^{-1}$ in the 16 energy points respectively.

*The work is partially supported by RFBR (Grants No 99-02-16813, 99-02-16815, 00-02-17478, 00-02-17481) and "Russian Universities" (Grant No 3H-339-00).

†email: V.N.Ivanchenko@inp.nsk.su

2 Data analysis

Main resonant background to the reaction (1) comes from the process

$$e^+e^- \rightarrow \phi \rightarrow \eta\gamma \rightarrow 3\pi^0\gamma \quad (2)$$

due to the merging of photons and/or loss of photons through the openings in the calorimeter. A smaller background comes from the decay mode [9]

$$e^+e^- \rightarrow \phi \rightarrow \eta\pi^0\gamma \quad (3)$$

Copiously produced $\phi \rightarrow K_S K_L \rightarrow \pi^0\pi^0 K_L$ events may contribute to the background but this decay is almost completely rejected by our cuts. The main source of non-resonant background is the process

$$e^+e^- \rightarrow \omega\pi^0 \rightarrow \pi^0\pi^0\gamma. \quad (4)$$

The QED background from e^+e^- annihilation into $4, 5\gamma$ was found negligible.

The data analysis was described in detail in our previous publications [4, 5]. In this work basically the same selection cuts were used requiring five isolated photons in the calorimeter with good shower profiles and event kinematics consistent with the $\pi^0\pi^0\gamma$ hypothesis (93 % c.l.). To suppress spurious photons from beams background all photons with energies less than 60 MeV at angles with respect to the beams less than 36 degrees were excluded from further analysis. The rate of events with spurious photons was about 4 % in PHI96 experiment and 8 % in PHI98. To account for this effect during processing of simulated events spurious hits, taken from the experiment, were admixed to Monte Carlo ones.

After applying cuts the sample of the $\pi^0\pi^0\gamma$ candidates was selected (Fig.1a). The main background is due to the process (4) but processes (2) and (3) contribute to this event sample also. The estimated number of events of the reaction (1) in Fig.1a is 419 ± 31 . The detection efficiency (Fig.1b) for the process (1) as a function of $\pi^0\pi^0$ invariant mass was determined using simulation of the process $\phi \rightarrow S\gamma \rightarrow \pi^0\pi^0\gamma$, where S is a scalar state with a mass ranging from 300 to 1000 MeV. The whole mass range was divided into 19 bins and within each bin simulation with uniform $m_{\pi\pi}$ distribution was performed. This simulation was used for determination of the $\pi^0\pi^0$ invariant mass resolution and event misidentification probabilities as well.

For the background process (4) the $\pi^0\gamma$ invariant mass distribution is peaked at ω -meson mass. The $m_{\pi\gamma}$ parameter is an invariant mass of the recoil photon and one of π^0 mesons, closest to the ω -meson mass (Fig.2). Events with

$$750 \text{ MeV} < m_{\pi\gamma} < 815 \text{ MeV} \quad (5)$$

are mainly ones of the process (4). Moreover in the energy range of the experiment $\pi^0\pi^0$ invariant mass in the process (4) must be lower than 700 MeV. For further analysis the selected $\pi^0\pi^0\gamma$ events were divided into three classes:

1. $m_{\pi\pi} < 700$ MeV and not (5);
2. $m_{\pi\pi} > 700$ MeV and not (5);

3. $m_{\pi\pi} < 700$ MeV and (5).

In the second class the $f_0\gamma$ mechanism dominates, in the third — the process (4).

For events of the second and third classes the experimental and simulated distributions in ψ and θ angles were compared. The ψ is an angle of the recoil photon with respect to pion direction in the $\pi^0\pi^0$ center of mass reference frame. The θ is an angle between recoil photon and the beam. It can be seen in Fig.3a,c that in the second class the distribution well matches one expected for the intermediate scalar state. Corresponding distributions in the third class agree with ones expected for the intermediate $\omega\pi^0$ state (Fig.3b,d).

3 Fitting of cross sections

The visible cross sections $\sigma_i(s)$ were measured for each energy point in both PHI96 and PHI98 experiments, here $s = 4E^2$ and i is a class number ($i=1,2,3$) defined above. These cross sections were fitted according to the following formulae:

$$\sigma_i(s) = \sum_{j=1,2} \alpha_{\pi\pi\gamma}^j(s) \epsilon_{\pi\pi\gamma}^{ij} \sigma_{\pi\pi\gamma}^j(s) + \alpha_{\eta\gamma}(s) \epsilon_{\eta\gamma}^i \sigma_{\eta\gamma}(s) + \alpha_{\eta\pi\gamma}(s) \epsilon_{\eta\pi\gamma}^i \sigma_{\eta\pi\gamma}(s) + \alpha_{\omega\pi}(s) \epsilon_{\omega\pi}^i \sigma_{\omega\pi}(s), \quad (6)$$

where $\sigma_{\pi\pi\gamma}^j(s)$ is a cross section for the j -th $m_{\pi\pi}$ interval ($j = 1$ for $m_{\pi\pi} < 700$ MeV, $j = 2$ for $m_{\pi\pi} > 700$ MeV), $\epsilon_{\pi\pi\gamma}^{ij}$ are probabilities for the $\pi^0\pi^0\gamma$ events belonging to j -th $m_{\pi\pi}$ interval to be detected as the class i events (Tabl.1,2), $\sigma_f(s)$ are production cross sections of the final state f ($f = \eta\gamma, \eta\pi^0\gamma, \omega\pi^0$), ϵ_f^i are detection efficiencies of the state f in the class i , $\alpha_f(s)$ — radiative corrections and corrections to the energy spread in the beam [10]. The expression for the $\sigma_{\eta\gamma}(s)$ was taken from Ref.[11], the values of the $\sigma_{\omega\pi}(s)$ as well as $\alpha_{\omega\pi}(s)$ were taken from our previous work [12]. The efficiencies $\epsilon_{\pi\pi\gamma}^{ij}$ were estimated using the experimental mass spectrum and the simulation of $S\gamma$ events described in the previous section. For the cross sections $\sigma_f(s)$ (f is $\pi^0\pi^0\gamma$ or $\pi^0\eta\gamma$) the following expression was used:

$$\sigma_f(s) = \frac{12\pi\Gamma_\phi^2 B(\phi \rightarrow ee) B(\phi \rightarrow R\gamma) m_\phi^3 F(s)}{s^{3/2} |D_\phi(s)|^2},$$

$$F(s) = \frac{\Gamma_{\phi R\gamma}(s)}{\Gamma_{\phi R\gamma}(m_\phi^2)}, \quad R = f_0, a_0.$$

Here the inverse propagator of ϕ was written according to Ref.[13]: $D_\phi(s) = m_\phi^2 - s - i \cdot \sqrt{s} \Gamma_\phi(s)$ and the energy dependence of partial widths $\Gamma_{\phi R\gamma}(s)$ was taken from Ref.[14]. The branching ratio of the decay (3) was obtained in SND work [9].

Note, that there is a dip in the cross section (4) at the ϕ -meson mass, due to destructive interference between the main non-resonance process, the $\phi \rightarrow \omega\pi^0$ decay, and the process

$$e^+e^- \rightarrow \phi \rightarrow \rho\pi^0 \rightarrow \pi^0\pi^0\gamma. \quad (7)$$

To check the accuracy of the detection efficiency, obtained by simulation, fully reconstructed events of the process (2) with 7 photons in the final state were analyzed. Since this process is similar to (1), the energy, invariant mass, and angular cuts were the same as in $\pi^0\pi^0\gamma$ analysis,

while threshold values for kinematic fitting parameters were scaled to provide same confidence level. Obtained branching ratio of the decay (2) was smaller than that from the SND experiment [11] $B(\phi \rightarrow \eta\gamma) = (1.338 \pm 0.053)\%$ by a factor of $\xi = 0.89 \pm 0.04$. This value was taken as a correction factor for both effect and background. This correction accounts for imprecise simulation of tails of distributions of parameters used in the cuts.

Free parameters of the fit were the branching ratios in the ϕ -meson peak $B(\phi \rightarrow \pi^0\pi^0\gamma)$ in two intervals of $m_{\pi\pi}$ (Tabl.1,2). Uncertainties in the values of Γ_ϕ , detection efficiencies, integrated luminosity, and energy spread of the beam were taken into account. The value of $B(\phi \rightarrow \eta\gamma)$ was fixed to its SND value, so our results are normalized to the branching ratio of the decay $\phi \rightarrow \eta\gamma$. The fitting results for both experiments are shown in the Table 3, corresponding curves for PHI98 are shown in Fig.4. Because the most of $\pi^0\pi^0\gamma$ events concentrate at high $m_{\pi\pi}$ similar analysis was performed for the mass range $m_{\pi\pi} > 900$ MeV.

4 Results

Because the fitting results for the PHI96 and PHI98 experiments are in a good agreement with each other (Tabl. 3) they was combined:

$$B(\phi \rightarrow \pi^0\pi^0\gamma) = (1.034 \pm 0.066 \pm 0.046) \cdot 10^{-4}, \quad m_{\pi\pi} > 700 \text{ MeV}, \quad (8)$$

$$B(\phi \rightarrow \pi^0\pi^0\gamma) = (0.559 \pm 0.053 \pm 0.025) \cdot 10^{-4}, \quad m_{\pi\pi} > 900 \text{ MeV}, \quad (9)$$

$$B(\phi \rightarrow \pi^0\pi^0\gamma) = (0.124 \pm 0.065 \pm 0.006) \cdot 10^{-4}, \quad m_{\pi\pi} < 700 \text{ MeV}. \quad (10)$$

In (8–10) the first error is statistical and the second one is systematic, which is determined mainly by current accuracy of $B(\phi \rightarrow \eta\gamma)$ (4 %) and model uncertainty (2 %) of $F(s)$ in the formula (7). From the data (8) and (10) one can evaluate the total value

$$B(\phi \rightarrow \pi^0\pi^0\gamma) = (1.158 \pm 0.093 \pm 0.052) \cdot 10^{-4}, \quad \phi \rightarrow \omega\pi^0 \text{ excluded}, \quad (11)$$

which is the total branching ratio excluding $\phi \rightarrow \omega\pi^0$ contribution, because the kinematic region of this decay is excluded by our cuts. It was studied in the SND work [15], from which one can obtain the branching ratio to the $\omega\pi^0$ region $B(\phi \rightarrow \pi^0\pi^0\gamma) = (0.063 \pm 0.031) \cdot 10^{-4}$ and add it to (11) to find the total branching ratio

$$B(\phi \rightarrow \pi^0\pi^0\gamma) = (1.221 \pm 0.098 \pm 0.061) \cdot 10^{-4}. \quad (12)$$

In this work the branching ratios were measured relatively to $B(\phi \rightarrow \eta\gamma)$. In such approach some systematic errors cancel allowing smaller total systematic uncertainties:

$$\begin{aligned} \frac{B(\phi \rightarrow \pi^0\pi^0\gamma)}{B(\phi \rightarrow \eta\gamma)} &= (0.913 \pm 0.073 \pm 0.029) \cdot 10^{-2}, \text{ total}; \\ \frac{B(\phi \rightarrow \pi^0\pi^0\gamma)}{B(\phi \rightarrow \eta\gamma)} &= (0.865 \pm 0.070 \pm 0.017) \cdot 10^{-2}, \omega\pi^0 \text{ excluded}; \\ \frac{B(\phi \rightarrow \pi^0\pi^0\gamma)}{B(\phi \rightarrow \eta\gamma)} &= (0.773 \pm 0.049 \pm 0.016) \cdot 10^{-2}, m_{\pi\pi} > 700 \text{ MeV}; \\ \frac{B(\phi \rightarrow \pi^0\pi^0\gamma)}{B(\phi \rightarrow \eta\gamma)} &= (0.418 \pm 0.040 \pm 0.009) \cdot 10^{-2}, m_{\pi\pi} > 900 \text{ MeV}. \end{aligned} \quad (13)$$

To investigate the dynamics of the reaction (1) the $\pi^0\pi^0$ invariant mass spectrum (Fig.1a) was studied in a narrower energy interval $2E = (1015 - 1025)$ MeV containing almost all ϕ -meson events and smaller $\omega\pi^0$ background. The estimated background from the processes (2–4) was subtracted using SND data [9, 12, 11]. Resulting raw mass spectrum is distorted due to finite detector resolution and misidentification of recoil photon in some $\pi^0\pi^0\gamma$ events. In order to obtain corrected spectrum the matrix $\epsilon_{i,j}$ was constructed, where each $\epsilon_{i,j}$ is a probability to get a reconstructed $m_{\pi\pi}$ value within the invariant mass bin i for an simulated event with actual $m_{\pi\pi}$ uniformly distributed in the bin j . Note, that in the two highest bins the simulated mass distribution were subdivided into smaller bins to take into account rapid decrease of the mass spectrum. The diagonal elements of the matrix and their immediate neighbors describe detector resolution. They turned out to be much larger than others which are due to misidentification of the recoil photon. Using this matrix and the experimental mass spectrum the number of events with misidentification were estimated and subtracted from each bin. This procedure does not affect the diagonal elements of the matrix and their immediate neighbors but zeroes all others.

After normalization to the total integrated luminosity and detection efficiency the differential branching ratios $S_{exp}(m_i) = dB(\phi \rightarrow \pi^0\pi^0\gamma)/dm_{\pi\pi}$ for both experiments were obtained. They are in a good agreement and thus can be combined together (Tabl.4). Using the matrix of efficiencies it is possible to restore the physical mass spectrum but such a procedure makes the values of corrected spectrum strongly correlated. To compare these results with model predictions one has to deal with a cumbersome covariance matrix. To simplify the analysis we instead transformed bare theory predictions $S_{th}(m)$ using the values of efficiencies from Table 4:

$$S_{cor}(m_i) = \epsilon_{i,i-1}S_{th}(m_{i-1}) + \epsilon_{i,i}S_{th}(m_i) + \epsilon_{i,i+1}S_{th}(m_{i+1}), \quad (14)$$

here $S_{cor}(m_i)$ is a corrected for the detector response theoretical mass spectrum, which should be used for approximation of the experimental spectrum $S_{exp}(m_i)$ by the least squares method. This approach is used in our fits, which are discussed in the next section.

5 Discussion

The $\pi^0\pi^0$ invariant mass spectrum (Fig.5) was approximated by the following function:

$$S_{th}(m) = S_{S\gamma}(m) + S_{\rho\pi}(m) + 2\sqrt{S_{S\gamma}(m)S_{\rho\pi}(m)} \cos \theta, \quad (15)$$

where $S_{S\gamma}(m)$ is the contribution of the $f_0\gamma$ and $\sigma\gamma$ decays, $S_{\rho\pi}(m)$ is the contribution of the process (7), and θ is an interference phase. This formula is exact only in case of identical angular distributions in $S\gamma$ and $\rho^0\pi^0$ intermediate states. Provided small $\rho^0\pi^0$ contribution, the difference in the angular distributions for the $\pi^0\pi^0\gamma$ final state can be approximately accounted for by fitting of θ . The $S_{\rho\pi}(m)$ dependence was taken from [14, 16]. Corresponding branching ratio is $B(\phi \rightarrow \rho\pi \rightarrow \pi^0\pi^0\gamma) = (1.2 \pm 0.2) \cdot 10^{-5}$ [16]. For $S_{S\gamma}(m)$ the expression from Ref.[14] was used

$$\begin{aligned} S_{S\gamma}(m) &= \frac{2m^2\Gamma_{\phi f\gamma}\Gamma_{f\pi^0\pi^0}}{\pi\Gamma_{\phi}} \left| \frac{1}{D_f(m)} + \frac{A}{D_{\sigma}(m)} \right|^2, \\ \Gamma_{f\pi^0\pi^0} &= \frac{g_{f\pi^+\pi^-}^2}{32\pi m} \sqrt{1 - \frac{4m_{\pi}^2}{m^2}}, \end{aligned} \quad (16)$$

where $D_S(m) = m_S^2 - m^2 + \Pi_S(m) - i \cdot m\Gamma_S(m)$ is f_0 or σ inverse propagator, $\Pi_S(m)$ takes into account finite width corrections [14], A is a complex parameter taking into account difference in coupling constants of f_0 and σ mesons.

In the kaon loop model of the $\phi \rightarrow f_0\gamma$ transition [14] $\Gamma_{\phi f\gamma}$ is proportional to the product $g_{fK^+K^-}^2 g_{f\pi^+\pi^-}^2$. The dependence of $\Gamma_{\phi f\gamma}$ on m in this model is different from the model with the point-like $\phi \rightarrow f_0\gamma$ transition and can be interpreted as a form factor, which stops the $\Gamma_{\phi f\gamma}$ growth at higher photon energies.

The free parameters of the fit were θ , A , m_f , and coupling constants $g_{fK^+K^-}$ and $g_{f\pi^+\pi^-}$ while the width and mass of the σ meson were fixed at $m_\sigma = 600$ MeV and $\Gamma_\sigma = 400$ MeV [17]. For σ meson the Breit-Wigner propagator with $\Pi_\sigma(m) = 0$ and $\Gamma_\sigma(m) = \text{const}$ was used. The fitting result is $A = -0.065_{-0.167}^{+0.083}$, indicating that $\sigma\gamma$ contribution is compatible with zero. This allows to reduce the number of free fitting parameters by fixing $A = 0$. For the remaining free parameters the following values were obtained:

$$\begin{aligned}
m_f &= (969.8 \pm 4.5) \text{ MeV}, \\
g_{fK^+K^-}^2/4\pi &= 2.47_{-0.51}^{+0.73} \text{ GeV}^2, \\
g_{f\pi^+\pi^-}^2/4\pi &= 0.54_{-0.08}^{+0.09} \text{ GeV}^2, \\
g_{fK^+K^-}^2/g_{f\pi^+\pi^-}^2 &= 4.6 \pm 0.8, \\
\theta &= (180 \pm 36) \text{ degrees}, \\
\chi^2/n_D &= 3/14.
\end{aligned} \tag{17}$$

Note, that although contribution from the process (7) is small, and fitting with this contribution set to zero still gives high confidence level ($\chi^2/n_D = 10/14$), but corresponding fitting curve (fig.5) shows visible systematic deviations from the observed mass spectrum.

The fitting results (17) demonstrate that the $f_0\gamma$ mechanism dominates in the decay (1), and contributions from $\sigma\gamma$ and $\rho^0\pi^0$ are small. Neglecting these contributions and assuming natural isotopic ratio $B(f_0 \rightarrow \pi^+\pi^-) = 2B(f_0 \rightarrow \pi^0\pi^0)$ one can obtain from (11)

$$\begin{aligned}
B(\phi \rightarrow f_0\gamma) &= (3.5 \pm 0.3_{-0.5}^{+1.3}) \cdot 10^{-4}, \\
\frac{B(\phi \rightarrow f_0\gamma)}{B(\phi \rightarrow \eta\gamma)} &= (2.6 \pm 0.2_{-0.3}^{+0.8}) \cdot 10^{-2}.
\end{aligned} \tag{18}$$

where the second errors are systematic which includes uncertainty in the interference terms. These errors were estimated by summation of systematic uncertainty from (11) and the difference between (18) and the value $B(\phi \rightarrow f_0\gamma) = 4.6 \cdot 10^{-4}$ calculated from (17) with $\sigma\gamma$ and $\rho^0\pi^0$ contributions taken into account.

The f_0 -meson width in the model [14] is a rapid function of m . At the resonance pole it is equal to $\Gamma_f(m_f) = -\text{Im}(D_f(m_f))/m_f = (201 \pm 28)$ MeV. Due to its close proximity to $K\bar{K}$ threshold this value is significantly larger than visible in Fig.5 f_0 width ~ 100 MeV. Note, that if the width corrections to the real part of f_0 propagator are set to zero the values of fitting parameters including f_0 mass and width change significantly: $m_f = 985_{-12}^{+16}$ MeV, $\Gamma_f = 122 \pm 13$ MeV, but such assumption looks much less attractive from the theoretical point of view. The model dependence of the f_0 mass and width explains disagreement between (17) and some data from PDG [18].

The model of Ref.[14] which takes into account the kaon loop contribution in the decay under study fits well the experimental spectrum. On the contrary, it is not possible to describe the data using the model with point-like transition mechanism, in which the transition form factor is equal to unity and $\Gamma_{\phi f_0 \gamma}$ is proportional to ω^3 , where ω is the photon energy. In this case the fitting curve does not follow the experimental spectrum and the $\chi^2/n_D = 28/14$ (fig.5). So, kaon loop contribution, which provides non point-like transition $\phi \rightarrow f_0 \gamma$ is confirmed by the our data.

The values of coupling constants (17) are in a good agreement with the 4-quark MIT bag model predictions [14, 19, 20]. New theoretical studies [21, 22, 23, 24, 25] were performed after first observation in order to explain the data. It was shown that it is possible to describe experimental results using different theoretical approaches. In these models the 4-quark component exists directly or “de facto” as a result of the kaon loops contribution.

6 Conclusion

Results of this work confirming our first publications [4, 5] and CMD-2 measurements [7] are based on the full SND data set which contains the largest statistics of $\pi^0 \pi^0 \gamma$ events. The shape of the $\pi^0 \pi^0$ mass spectrum is described well by the sum of $\rho \pi$ and $f_0 \gamma$ contributions. The contribution of $\sigma \gamma$ intermediate state is not required for description of the data but is not completely excluded by our data. It is shown that point-like transition model does not fit the experimental mass spectrum. At the same time, models with intermediate kaon loops reproduce the data. Predictions of the four-quark MIT bag model of the f_0 meson are in a good agreement with our results but we cannot exclude other explanations. Further theoretical studies and new data are needed to obtain consistent description of the $f_0(980)$ -meson quark structure and to detect $\sigma \gamma$ contribution in the $\phi \rightarrow \pi^0 \pi^0 \gamma$ decay.

7 Acknowledgments

Authors are grateful to N.N.Achasov for useful discussions and valuable comments.

References

- [1] V.P.Druzhinin et al., Z.Phys. **C 37**, 1 (1987).
- [2] S.I.Dolinsky et al., Phys. Reports **202**, 99 (1991).
- [3] M.N.Achasov et al., In: Proc. of HADRON’97, Upton, NY, 25-30 Aug 1997, p.26; e-Print Archive: hep-ex/9710017.
- [4] M.N.Achasov et al., Phys. Atom. Nucl. **62**, 442 (1999); Yad. Fiz. **62**, 484 (1999).
- [5] M.N.Achasov et al., Phys. Lett. **B440**, 442 (1998).
- [6] M.N.Achasov et al., Nucl. Inst. Meth. **A**, (2000); Preprint IYF 99-76, Novosibirsk, 1999.

- [7] R.R.Ahmetshin et al., Phys. Lett. **B462**, 380 (1999).
- [8] M.N.Achasov et al., Budker INP 98-65, Sep 1998; e-Print Archive: hep-ex/9809013.
- [9] M.N.Achasov et al., Phys. Lett. **B438**, 441 (1998).
- [10] M.N.Achasov et al., Jour. Exp. Theor. Phys. **90**, (2000).
- [11] M.N.Achasov et al., Eur. Phys. J. **C12**, 25 (2000).
- [12] D.A.Bukin et al., Preprint INP 99-103, Novosibirsk, 1999.
- [13] N.N.Achasov et al., Sov. J. Nucl. Phys. **54**, 664 (1991); Int. J. Mod. Phys. **A7**, 3187 (1992).
- [14] N.N.Achasov, V.N.Ivanchenko, Nucl. Phys. **B 315**, 465 (1989).
- [15] M.N.Achasov et al., Nucl. Phys. **B569**, 158 (2000).
- [16] A.Bramon, A.Grau, G.Panchieri, Phys. Lett. **B 283**, 416 (1992).
- [17] M.Ishida et al., Proc. Workshop on Hadron Spectroscopy, Frascati, March 8-12, 1999, p.115, e-Print Archive: hep-ph/9905261.
- [18] C.Caso et al. (Particle Data Group) Europ. Phys. Jour. **C 3**, 1 (1998).
- [19] R.L.Jaffe, Phys. Rev. **D 15**, 267, 281 (1977).
- [20] N.N.Achasov, Phys. Usp. **41**, 1149 (1998); Usp. Fiz. Nauk **168**, 1257 (1998).
- [21] R.Delbourgo, Dongsheng Liu, M.D.Scadron, Phys. Lett. **B446**, 332 (1999).
- [22] E.Marco et al., Phys. Lett. **B470**, 20 (1999).
- [23] V.E.Markushin, M.P.Locher, In: Proc. of Work. on Hadron Spectroscopy, Frascati, March 8-12, 1999, p.229, e-Print Archive: hep-ph/9906249.
- [24] J.L.Lucio, M.Napsuciale, In: Proc. 3rd Workshop on Physics and Detectors for DAΦNE, Frascati, Nov. 16-19, 1999, e-Print Archive: hep-ph/0001136.
- [25] N.A.Tornqvist, Eur. Phys. Jour. **C11**, 359 (1999).

Table 1: The matrix of detection efficiencies for three classes of events for the PHI96 experiment.

j	1	2
$m_{\pi\pi}, \text{ MeV}$	300–700	700–1000
$\epsilon_{\pi\pi\gamma}^{1j}, \%$	13.27	0.82
$\epsilon_{\pi\pi\gamma}^{2j}, \%$	1.46	18.25
$\epsilon_{\pi\pi\gamma}^{3j}, \%$	5.11	0.45

Table 2: The matrix of detection efficiencies for three classes of events for the PHI98 experiment.

j	1	2
$m_{\pi\pi}, \text{ MeV}$	300–700	700–1000
$\epsilon_{\pi\pi\gamma}^{1j}, \%$	14.34	0.87
$\epsilon_{\pi\pi\gamma}^{2j}, \%$	1.79	18.87
$\epsilon_{\pi\pi\gamma}^{3j}, \%$	4.19	0.47

Table 3: The results of the fit of the cross sections.

Experiment	PHI96	PHI98
$B(\phi \rightarrow \pi^0 \pi^0 \gamma) \cdot 10^4, m_{\pi\pi} < 700\text{MeV}$	0.258 ± 0.111	0.055 ± 0.080
$B(\phi \rightarrow \pi^0 \pi^0 \gamma) \cdot 10^4, m_{\pi\pi} > 700\text{MeV}$	0.960 ± 0.102	1.087 ± 0.086
$B(\phi \rightarrow \pi^0 \pi^0 \gamma) \cdot 10^4, m_{\pi\pi} > 900\text{MeV}$	0.582 ± 0.085	0.545 ± 0.068

Table 4: The $m_{\pi\pi}$ mass bins, average mass inside the bin m_i , the non zero elements of the efficiency matrix $\epsilon_{i,j}$, and the normalized experimental invariant mass spectrum for the $\phi \rightarrow \pi^0\pi^0\gamma$ decay after background subtraction and acceptance corrections. Only statistical error are shown. Systematic uncertainty is 4.5 %.

N	$m_{\pi\pi}$, MeV	m_i , MeV	$\epsilon_{i-1,i}$	$\epsilon_{i,i}$	$\epsilon_{i+1,i}$	$\frac{dB(\phi \rightarrow \pi^0\pi^0\gamma)}{dm_{\pi\pi}} \cdot 10^8$ (MeV $^{-1}$)
1	300-400	350	-	0.953	0.047	3.36 ± 4.47
2	400-500	450	0.037	0.920	0.043	1.01 ± 4.67
3	500-600	550	0.043	0.900	0.056	1.94 ± 3.11
4	600-700	650	0.042	0.718	0.240	6.26 ± 2.00
5	700-720	710	0.058	0.660	0.281	9.46 ± 6.46
6	720-740	730	0.227	0.536	0.237	13.99 ± 6.14
7	740-760	750	0.221	0.544	0.235	13.53 ± 6.07
8	760-780	770	0.240	0.537	0.223	18.23 ± 6.26
9	780-800	790	0.242	0.546	0.212	16.93 ± 6.08
10	800-820	810	0.221	0.558	0.220	24.04 ± 7.36
11	820-840	830	0.233	0.559	0.208	28.07 ± 7.65
12	840-860	850	0.223	0.572	0.205	26.59 ± 7.59
13	860-880	870	0.215	0.564	0.221	34.15 ± 8.28
14	880-900	890	0.202	0.613	0.185	44.37 ± 9.37
15	900-920	910	0.192	0.630	0.179	43.15 ± 8.95
16	920-940	930	0.197	0.651	0.153	61.66 ± 10.38
17	940-960	950	0.171	0.698	0.131	65.45 ± 10.71
18	960-980	969	0.178	0.728	0.095	70.14 ± 12.61
19	980-1000	987	0.214	0.786	-	30.52 ± 10.08

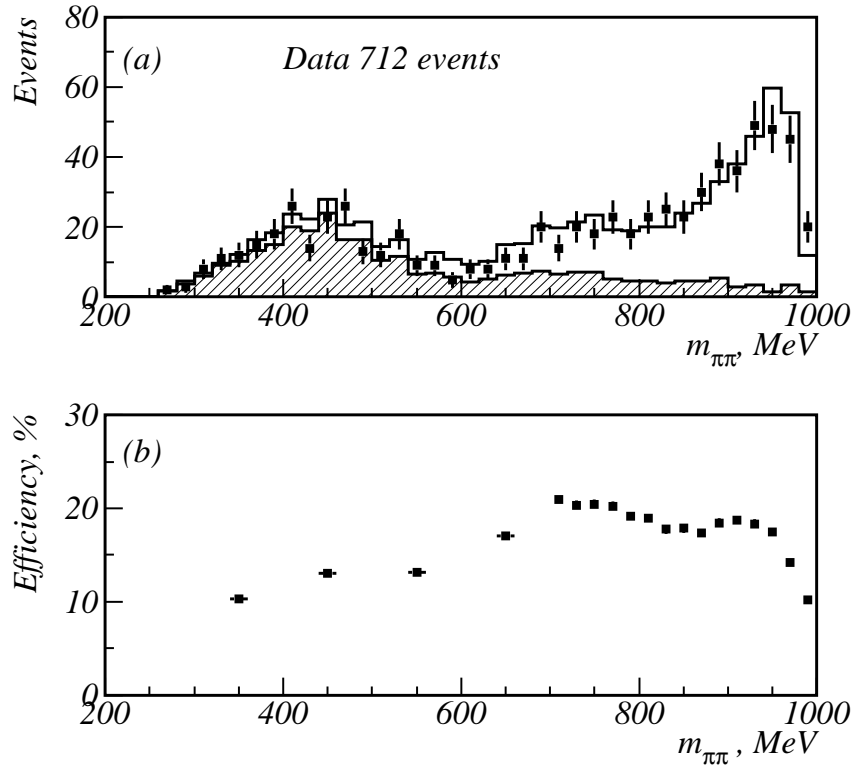


Figure 1: The mass spectra for $\pi^0\pi^0\gamma$ events: a — the invariant mass distribution of $\pi^0\pi^0$ pairs without acceptance corrections, beam energy $1015 \text{ MeV} < 2E < 1025 \text{ MeV}$, histogram — data, shaded histogram — estimated background; b — the detection efficiency for the process $e^+e^- \rightarrow S\gamma \rightarrow \pi^0\pi^0\gamma$, S is a scalar state.

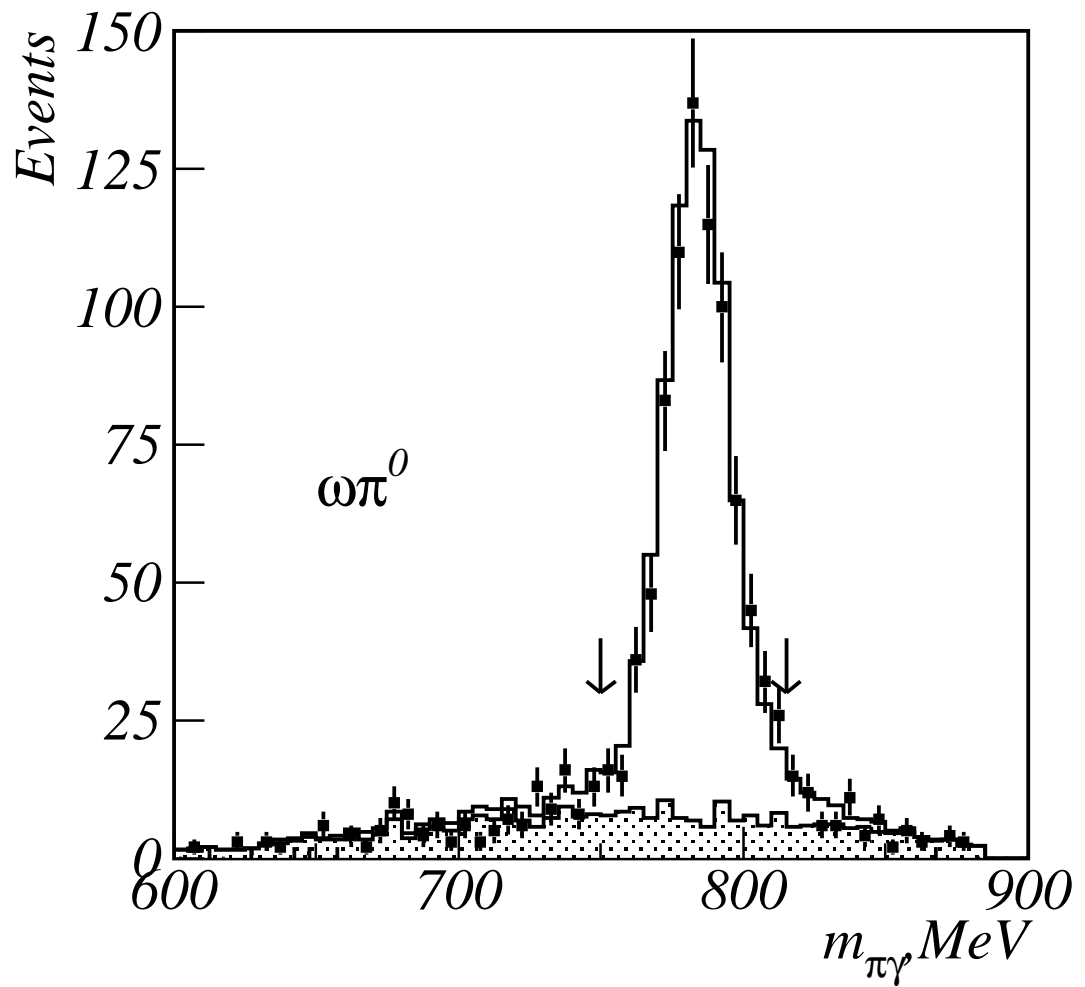


Figure 2: Distribution of $\pi^0\gamma$ invariant mass for $m_{\pi\pi} < 700$ MeV. Points — data, histogram — simulation, shaded histogram — sum of contributions from the ϕ decays, arrows — selection of $\omega\pi^0$.

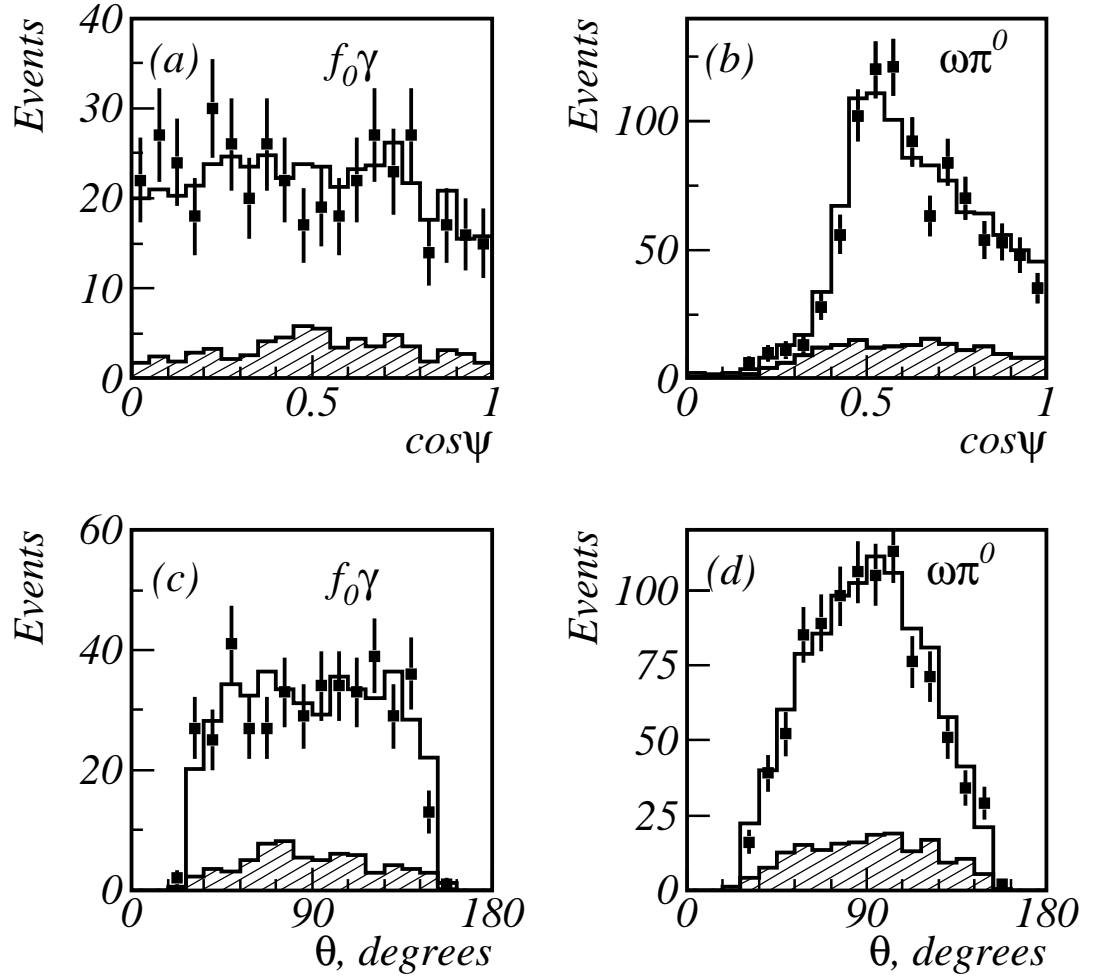


Figure 3: The angular spectra for $\pi^0\pi^0\gamma$ events: a, b — distribution of cosine of ψ , the angle between directions of π^0 and recoil γ in the rest frame of $\pi^0\pi^0$ system; c, d — distributions of θ , angle of the recoil γ with respect to the beam. Points — data, histogram — simulation, shaded histogram — sum of contributions from background processes for the reaction (1) (a,c) and for (4) (b,d). Acceptance corrections are not applied. Beam energy is $1015 \text{ MeV} < 2E < 1025 \text{ MeV}$.

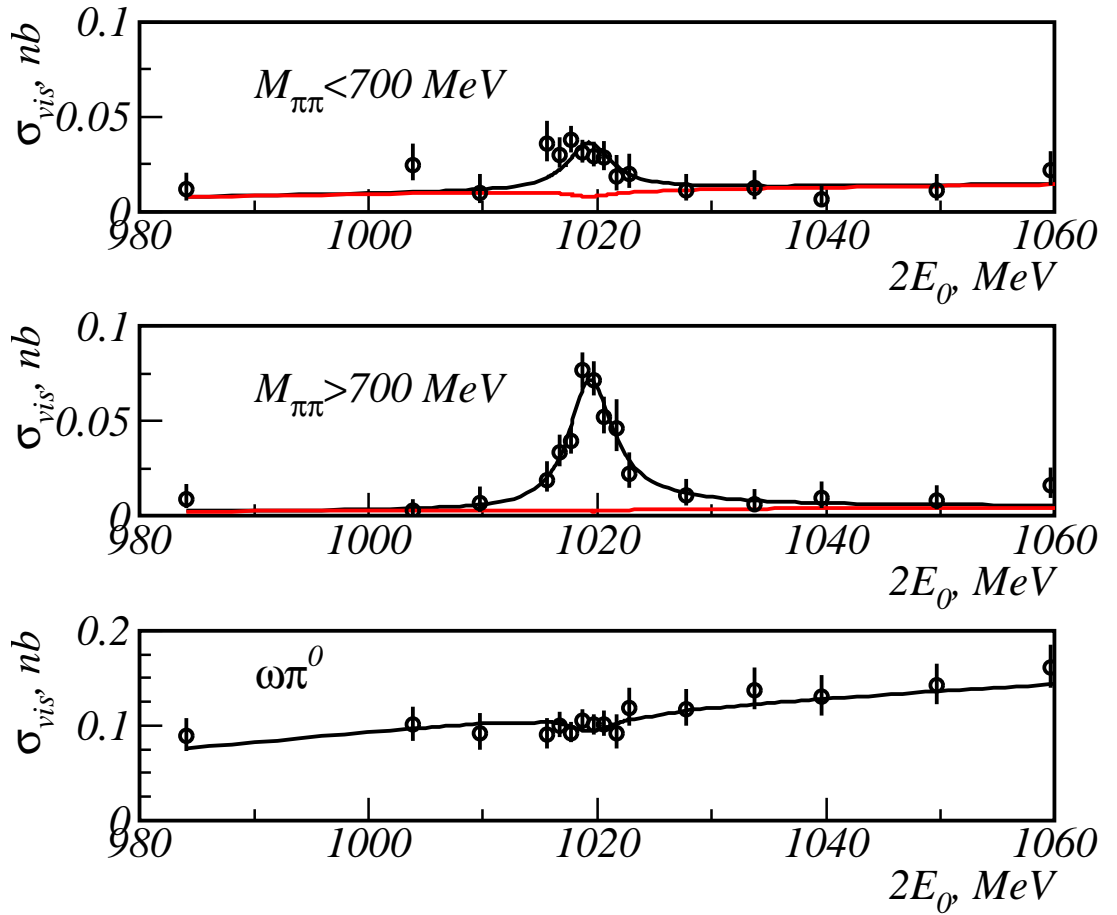


Figure 4: Energy dependence of the visible $e^+e^- \rightarrow \pi^0\pi^0\gamma$ cross section for the three classes of events described in the text for the PHI98 experiment. Points — data, solid line — fit, dotted line — sum of background contributions to the decay $\phi \rightarrow \pi^0\pi^0\gamma$.

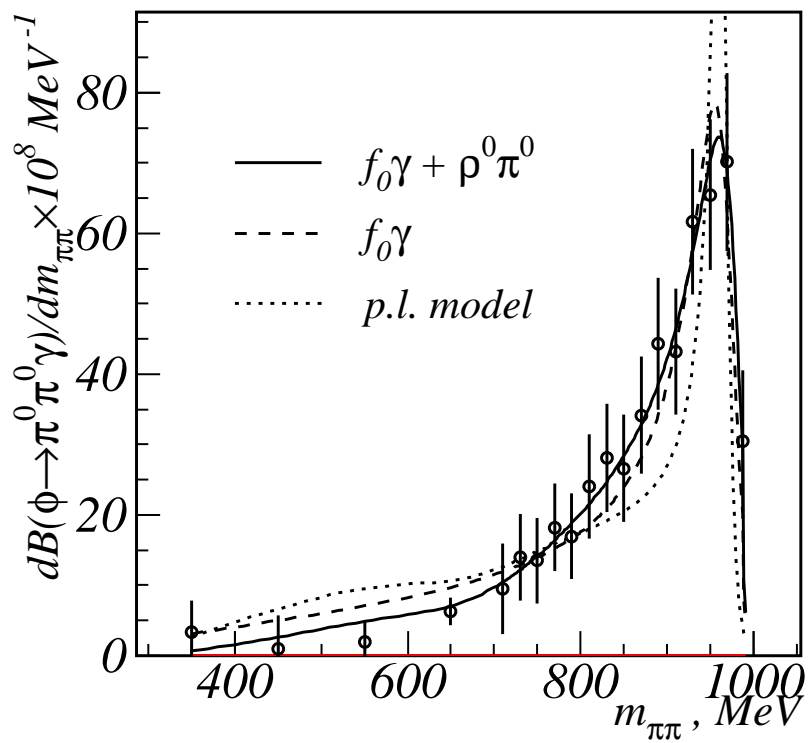


Figure 5: The $\pi^0\pi^0$ invariant mass spectrum after background subtraction and acceptance corrections: points — data, solid line — the result of the fit, dashed line — the result of the fit without $\rho^0\pi^0$ contribution; dotted line — the result of the fit in the point-like transition model.